

Nanometric skyrmion lattice from anisotropic exchange interactions in a centrosymmetric host

Max Hirschberger^{1,2,*}, Satoru Hayami¹, Yoshinori Tokura^{1,2,3}

¹*Department of Applied Physics and Quantum-Phase Electronics Center,
The University of Tokyo, Bunkyo-ku, Tokyo 113-8656, Japan*

²*RIKEN Center for Emergent Matter Science (CEMS), Wako, Saitama 351-0198, Japan*

³*Tokyo College, The University of Tokyo,
Bunkyo-ku, Tokyo 113-8656, Japan*

(Dated: March 25, 2025)

Abstract

Skyrmion formation in centrosymmetric magnets without Dzyaloshinskii-Moriya interactions was originally predicted from unbiased numerical techniques. However, no attempt has yet been made, by comparison to a real material, to determine the salient interaction terms and model parameters driving spin-vortex formation. We identify a Hamiltonian with anisotropic exchange couplings, local ion anisotropy, and four-spin interactions, which is generally applicable to this class of compounds. In the representative system $\text{Gd}_3\text{Ru}_4\text{Al}_{12}$, anisotropic exchange drives a fragile balance between helical, skyrmion lattice, and transverse conical (cycloidal) orders. The model is severely constrained by the experimentally observed collapse of the SkL with a small in-plane magnetic field. For the zero-field helical state, we further anticipate that spins can be easily rotated out of the spiral plane by a tilted magnetic field or applied current.

INTRODUCTION

The modern push to realize complex magnetism with strong coupling to the electronic degrees of freedom is underpinned, to a large extent, by ever more powerful computational techniques. Amongst these are unbiased numerical simulations, such as Monte-Carlo methods, for magnetic ground states, excitation spectra, and spin dynamics starting from an (effective) spin-spin Hamiltonian. Monte-Carlo studies originally predicted that centrosymmetric triangular lattice magnets, be they insulators with (superexchange) interactions^{1,2} or metals with effective Ruderman-Kittel-Kasuya-Yosida (RKKY) couplings³⁻⁵, can host nanometer-sized magnetic spin vortices with net topological charge (i.e., skyrmions), and a multitude of even more complex states^{3,6,7}. The theoretical work has introduced a new playground for the application of concepts from topology in condensed matter, but only with the observation of skyrmion lattices in the hexagonal intermetallics Gd_2PdSi_3 ⁸ and $\text{Gd}_3\text{Ru}_4\text{Al}_{12}$ ⁹ has a more systematic comparison of theory and experiment become possible.

In this article, we demonstrate via a combination of theory and experiments that moderately weak anisotropic exchange from dipolar and spin-orbit interactions is sufficient to realize the skyrmion lattice state in centrosymmetric magnets. Anisotropic exchange hence represents a new, third avenue towards the SkL in bulk crystals with inversion center, beyond frustrated exchange and higher-order RKKY interactions. Next to the present focus

on intermetallic systems, this notion may have implications also for spin-vortex formation in insulating materials, e.g. on the magnetic diamond lattice of MnSc_2S_4 ^{10,11}. In non-centrosymmetric magnets and at interfaces, spin-orbit coupling (SOC) provides the crucial underpinning of spin-spiral and skyrmion formation via the Dzyaloshinskii-Moriya interaction^{12–15}. Likewise, we here show that SOC can play an important role in centrosymmetric magnets with SkL, as a driver of anisotropic exchange. Our work on weakly anisotropic exchange also creates a conceptual link between SkL formation and the movement to realize new quantum-disordered states in frustrated magnets via strongly bond-anisotropic exchange^{16,17}.

The focus of our study is $\text{Gd}_3\text{Ru}_4\text{Al}_{12}$, a representative of the new class of centrosymmetric skyrmion hosts with coupled local moments and itinerant electrons. The Gd^{3+} magnetic moments in this structure are arranged in quasi-layered Kagome nets, which are distorted by alternate stretching and compression of Kagome bond distances^{18–20} – termed breathing Kagome lattice [Fig. 1(a)]. The magnetic phase diagram for field along the crystallographic c -axis (perpendicular to the Kagome plane) harbors five distinct regimes^{9,21}: Helical order (HE), a Transverse Conical state (TC), fan-like order (F), the skyrmion lattice (SkL), and the as-yet uncharacterized pocket labeled by the Roman numeral V [Fig. 1(b)]. In our analysis, a key guiding factor for the numerical simulation is the stability range of the SkL as compared to TC.

MODEL HAMILTONIAN

Motivated by the structural feature of rare earth triangles, and by previous considerations of the specific heat²², we approximately treat $\text{Gd}_3\text{Ru}_4\text{Al}_{12}$ as a two-dimensional triangular lattice of strongly coupled superspin trimers [small triangles in the projection plane of Fig. 1(a)]. Figure 1(b) shows that the zero-field magnetic ground state of hexagonal $\text{Gd}_3\text{Ru}_4\text{Al}_{12}$ is a spiral, where the magnetic modulation vector \mathbf{q} is aligned within the basal plane. In fact, three \mathbf{q}_ν with $\nu = 1, 2, 3$ must be degenerate by symmetry, and previous work has shown that the \mathbf{q}_ν point along the a^* axis and equivalent directions^{9,21}. Backed by the knowledge that the directors $\hat{\mathbf{q}}_\nu$ are identical in all phases experimentally studied so far, we choose a minimal Hamiltonian consistent with the six-fold symmetry of the lattice and suitable for discussion of the magnetic phase transitions²³. Only the dominant Fourier components $\mathcal{S}_{\mathbf{q}_\nu}^\alpha$

of the local spin \mathbf{S}_i at lattice site i are carried over²⁴, so that

$$\begin{aligned} \mathcal{H}/J = & 2 \sum_{\nu} [-\mathcal{H}_{\nu} + (K/N) (\mathcal{H}_{\nu})^2] \\ & - A \sum_i (\mathcal{S}_i^z)^2 - h \sum_i \hat{\mathbf{h}} \cdot \mathbf{S}_i \end{aligned} \quad (1)$$

with $\mathcal{H}_{\nu} = \sum_{\alpha,\beta} \Gamma_{\mathbf{q}_{\nu}}^{\alpha\beta} \mathcal{S}_{\mathbf{q}_{\nu}}^{\alpha} \mathcal{S}_{-\mathbf{q}_{\nu}}^{\beta}$. Here, J is the energy scale for the dominant two-spin interaction, while (K/N) , A , and h are dimensionless parameters corresponding to the strength of four-spin interaction, local ion anisotropy, and external magnetic field, respectively (normalized by J in all three cases). N is the number of spins in the system, and the direction of the applied magnetic field is labeled as $\hat{\mathbf{h}}$. The matrices $\Gamma_{\mathbf{q}_{\nu}}^{\alpha\beta}$ are also dimensionless and characterize the anisotropic exchange interactions. For example for $\nu = 1$, we have $\Gamma_{\mathbf{q}_1} = \text{diag}(I_0 - I_{\text{ani}}, I_0 + I_{\text{ani}}, I_z)$; the other $\Gamma_{\mathbf{q}_{\nu}}$ are obtained from $\Gamma_{\mathbf{q}_1}$ by a simple rotation operation of $\pm 120^\circ$. In contrast to models of magnetic interactions in real space, the present (momentum-space) approach for the two-spin and four-spin terms is not sensitive to the choice of boundary conditions²⁵. For simplicity of the numerical treatment, the calculations were carried out for \mathbf{q}_{ν} rotated by 90° from those in Fig. 1(c), i.e. for \mathbf{q}_{ν} along the triangular lattice's bond direction.

Anisotropic interactions of the I_{ani} -type can be caused by relativistic spin-orbit coupling²³, but we note that dipolar interactions at the nearest neighbor level are also included in this term. In Discussion, we comment on the prospect of fully ab-initio calculations of I_{ani} in this class of compounds. More broadly speaking, Hamiltonians analogous to Eq. (1) are believed to be a good starting point as well for the description of phase transitions in centrosymmetric metallic magnets of different symmetries, such as tetragonal or cubic, if the \mathbf{q}_{ν} are strongly pinned to preferred crystal axes. Moreover, the formalism can be adapted to the description of non-centrosymmetric materials²⁶ by inclusion of antisymmetric terms $\Gamma_{\mathbf{q}_{\nu}}^{\alpha\beta} \neq \Gamma_{\mathbf{q}_{\nu}}^{\beta\alpha}$, although this implies a larger number of adjustable parameters. When allowing for moderate (%-scale) changes of the modulus $q_{\nu} = |\mathbf{q}_{\nu}|$ at phase boundaries — including transitions from orders incommensurate with the underlying crystal lattice, to commensurate ones — the energy landscape is modified but weakly due to the typically very broad magnetic susceptibility (Lindhard function) $\chi(\mathbf{q})$ in metallic magnets with large, localized magnetic moments²⁷.

Without loss of generality, $I_z = I_0 = 1$ is used in the following, as small differences between I_0 and I_z can be absorbed into A , where large (small) I_z corresponds to positive

(negative) A . Previous magnetization measurements indicated mild easy-plane anisotropy $A < 0$ of local ions in $\text{Gd}_3\text{Ru}_4\text{Al}_{12}$ ^{9,22}. As $A < 0$ favors the transverse conical state (TC) already in zero magnetic field, $I_{\text{ani}} > 0$ is crucial to obtain phase HE with spiral vectors $\mathbf{q}_\nu \parallel a^*$ at $h = 0$. In other words, stronger interactions parallel to the direction of the bond between triangular lattice sites are necessary to obtain phase HE in the present compound [Fig. 1(c)].

Detailed supporting calculations show that excess I_{ani} strongly favors multi- \mathbf{q} phases, promoting the SkL over TC at all temperatures and eventually causing an instability of HE towards a multi- \mathbf{q} state²⁸. To describe $\text{Gd}_3\text{Ru}_4\text{Al}_{12}$, we focus on $0 < I_{\text{ani}} < 0.1$ and set $K = 0$, the latter choice being revisited below. Within this range of parameters, the phase boundaries at $\hat{\mathbf{h}} \parallel c$ are rather robust. For example, the simulations demonstrate that in absence of single ion anisotropy ($A = 0$), the overall properties of the c -axis phase diagram are nearly unchanged as compared to $(I_{\text{ani}}, A) = (0.01, -0.007)$. As we will show now, a good match of experiment and theory is obtained for $I_{\text{ani}} = 0.01$ and $A = -0.007$, especially when aiming to also describe the case of $\hat{\mathbf{h}}$ tilted away from the c -axis.

UNBIASED MODELING OF MAGNETIC PHASE TRANSITIONS FOR $\hat{\mathbf{h}} \parallel c$

Figure 2(a) shows the components $S_\alpha(\mathbf{q}_\nu)$ of the calculated magnetic structure factor, which is proportional to the squared Fourier component of the magnetic moment $m_\alpha(\mathbf{q}_\nu)^2$. We use $S_\alpha(\mathbf{q}_\nu)$ and $m_\alpha(\mathbf{q}_\nu)^2$ interchangeably in the following. Here, the indices $\alpha = \parallel, \perp, z$ relate to a Cartesian frame of reference with unit vectors $\mathbf{e}_{\parallel\nu} = \hat{\mathbf{q}}_\nu$, $\mathbf{e}_{z\nu} = \hat{z}$, and $\mathbf{e}_{\perp\nu}$ perpendicular to both. For convenience, we also define $m_{xy}^2 = m_\parallel^2 + m_\perp^2$. For the chosen model parameters, the zero-field ground state corresponds to a helical spiral (HE) with $\mathbf{q} = \mathbf{q}_1$ [Fig. 2(d,g)] with very weak admixtures of fan-like components at $\mathbf{q}_2, \mathbf{q}_3$ ²⁸. When $\hat{\mathbf{h}}$ is applied parallel to the c -axis, the system transitions into a TC state (only $m_{xy} \neq 0$ for a single \mathbf{q}_ν), then to the SkL ($m_{xy} \neq 0, m_z \neq 0$ with equal weight for all three \mathbf{q}_ν), back into the TC phase, and finally into a high-field order which can be either transverse conical or fan-like, depending on the exchange parameters²⁸. Sharp changes in $S_\alpha(\mathbf{q}_\nu)$ indicate first order phase transitions, which bound the SkL state and also characterize the spin-flop transition between HE and TC. Experimentally, these transitions were found to be accompanied by strong hysteresis. The strong history dependence of the experimental

observations in phase TC, c.f. Fig. 1(b) and Ref.⁹, in fact represents a challenge for the comparison to the theoretical result [Fig. 2(a,b)]. We discuss agreement of the two phase diagrams in more detail in the Supplementary Information²⁸.

EXPERIMENT: DESTRUCTION OF SKYRMION LATTICE WITH IN-PLANE MAGNETIC FIELD

The general characteristics of the calculated phase diagram for $\hat{\mathbf{h}} // c$ are unchanged for a rather broad range of Hamiltonian parameters as long as $I_{\text{ani}} > 0 > A$ and $I_{\text{ani}} + A \geq 0$ ²⁸. To further constrain the two free parameters A and I_{ani} , we experimentally studied the effect of tilting the magnetic field away from c by an angle θ , c being the direction of six-fold symmetry (Fig. 3). We hence establish that in $\text{Gd}_3\text{Ru}_4\text{Al}_{12}$, the critical angle θ_c of the skyrmion lattice phase is only $10 - 15^\circ$. In the experiment, we use the Hall conductivity σ_{xy} as a sensor for the SkL phase. This observable is the transverse element of the conductivity tensor $\sigma_{\alpha\beta}$ relating electric field E_α and resulting charge current via $J_\alpha = \sigma_{\alpha\beta} E_\beta$. The Hall conductivity acquires an additional contribution in the SkL phase, the topological Hall effect (THE), which effectively measures the winding number of a single skyrmion²⁹⁻³¹. In our measurements of angle-dependent σ_{xy} , the THE emerges as a bell-shaped anomaly on top of a smooth background.

Outside the SkL phase, the curves of $\sigma_{xy}(\theta)$ collapse nicely onto a cosine-shaped profile. This behavior is consistent with the understanding that the oscillating background, on top of which the topological Hall signal $\sigma_{xy}^{\text{T}} \approx 250 \Omega^{-1} \text{cm}^{-1}$ of the SkL develops, is due to spin-orbit coupling and the Karplus-Luttinger type anomalous Hall effect σ_{xy}^{KL} ^{32,33}. For σ_{xy}^{KL} , temperature dependence is not expected as long as the conduction electron's spin polarization remains unchanged³⁴. Moreover, σ_{xy}^{KL} is proportional to the c -component of the net magnetization, consistent with the cosine-law observed here³².

The experimental σ_{xy} data is reported as a function of the applied magnetic field $\mu_0 H$ in units of Tesla, where μ_0 is the vacuum permeability. We corrected for the demagnetization effect by determining the internal field $\mu_0 H_{\text{int}} = \mu_0 (H - NM)$, where M is the magnetization per unit volume, measured independently, and $0 \leq N \leq 1$ is the demagnetization factor calculated in elliptical approximation²⁸. Given the presence of Gd^{3+} ions with a moment of seven Bohr magneton (μ_B) in this material, the corresponding dimensionless Zeeman energy

is $h = 7\mu_B \cdot (\mu_0 H_{\text{int}})/J^{28}$.

The present experimental observations contrast previous findings on the far more stable skyrmion lattice with larger $\theta_c \sim 45^\circ$ in the related hexagonal compound Gd_2PdSi_3 , with a triangular net of rare earth moments⁸. In $\text{Gd}_3\text{Ru}_4\text{Al}_{12}$, the delicate interplay between TC and SkL for $\mathbf{H} \parallel c$, and also the low value of θ_c , are both consequences of a fine balance between the parameters A and I_{ani} .

MODELING THE PHASE DIAGRAM IN TILTED FIELD

Let the in-plane component of $\hat{\mathbf{h}}$ be aligned along \mathbf{q}_1 . We use the simulated annealing framework to first discuss the character of magnetic order above the critical angle θ_c . Figures 4(a,b) show how only a single modulation direction, \mathbf{q}_1 , survives under these conditions, with spins arranged in a conical fashion around the axis $\hat{\mathbf{n}}$. In the simulation, $\hat{\mathbf{n}} \parallel \hat{\mathbf{h}}$ in this regime, so that the conical axis rotates smoothly as θ is changed. The resulting dependences $m_{\parallel}^2 \sim \cos^2 \theta$ and $m_z^2 \sim \sin^2 \theta$ are indicated by black solid lines in Fig. 4(a).

We are now in a position to explore the parameter range of I_{ani} and A suitable to describe the experimental situation in $\text{Gd}_3\text{Ru}_4\text{Al}_{12}$, when using the trimer approximation (Fig. 5). The calculations demonstrate that for each $I_{\text{ani}} > 0$ there is a critical A_c which separates the stability regime of two zero-field ground states: For $A > A_c$, a helical spiral is the preferred spin configuration, but it succumbs to the transverse conical state when $A < A_c$. Figure 5 shows the A_c values as dashed vertical lines for $I_{\text{ani}} = 0.01, 0.02, 0.03$. The key point here is that only for small $I_{\text{ani}} = 0.01 - 0.02$, the critical angle θ_c of the skyrmion lattice can be continuously tuned to zero before the collapse of the zero-field HE state. Following Fig. 5, we conclude that the experimental situation in $\text{Gd}_3\text{Ru}_4\text{Al}_{12}$ is well described using the trimer approximation and $0 < I_{\text{ani}} < 0.02$ with correspondingly small, finely tuned A .

We return to a question which was postponed earlier: What is the role of the four-spin term K in Eq. (1), or rather: could $K \neq 0$ explain the experiments for $\text{Gd}_3\text{Ru}_4\text{Al}_{12}$? K is well known to strongly favor multi- \mathbf{q} order such as the skyrmion lattice⁴, and it comes as no surprise that $K > 0$ enhances the critical angle θ_c for a variety of combinations of (A, I_{ani}) . For example when $I_{\text{ani}} = 0.01$ and $K = 0.03$, the skyrmion lattice is stable even when $\hat{\mathbf{h}}$ is fully aligned along the in-plane direction x . As this is inconsistent with the observed small critical angle, we maintain that $K = 0$ is suitable for the present breathing Kagome

compound.

DISCUSSION

Many previous numerical studies have relied on Heisenberg Hamiltonians which yield, in a certain parameter range, a SkL phase when aided by thermal fluctuations or easy-axis anisotropy $A > 0$ ^{1,2,35}. These models are not well suited to the present material, where the SkL is realized despite $A < 0$. Likewise, RKKY Hamiltonians with biquadratic interactions ($K \neq 0$)^{3,4} are inconsistent, in our simulations, with the very small critical angle θ_c observed experimentally for $\text{Gd}_3\text{Ru}_4\text{Al}_{12}$. Hence, a new approach, emphasizing the role of anisotropic exchange $I_{\text{ani}} > 0$ together with easy-plane anisotropy of rare earth ions, is used to model the stability ranges of helical, transverse conical, and SkL phases on the triangular lattice of superspin trimers, corresponding to the trimerized limit of the breathing Kagome network in $\text{Gd}_3\text{Ru}_4\text{Al}_{12}$ ^{21,22}. Spin-orbit coupling²³ and next-neighbor dipolar interactions both contribute to I_{ani} . Note that easy-plane single-ion anisotropy was previously thought to be detrimental to skyrmion formation in magnets with inversion center^{2,35}. However, $A < 0$ can stabilize Neel skyrmions in noncentrosymmetric polar materials^{36,37}.

The prediction of I_{ani} for itinerant electron systems through fully ab-initio electronic structure calculations remains an open challenge in this field. I_{ani} is expected to be strongly dependent on the shape of Fermi surface sheets, as well as on the atomic spin-orbit coupling parameter λ_{SOC} of the orbitals constituting the conduction bands.

It is worth reiterating that the conical axis $\hat{\mathbf{n}}$ in $\text{Gd}_3\text{Ru}_4\text{Al}_{12}$ may be easily tilted away from being parallel to \mathbf{q} (Figs. 4, 5). This experimental condition has potential applications in the field of reading and writing skyrmions by very weak external perturbations. Our study also indicates that depinning of the skyrmion lattice using an applied DC electrical current should be achievable in this material class.

A recent focus of research on spiral magnets is the detection of the emergent electric field resulting from spin dynamics driven by electrical currents, i.e. the realization of an emergent (or quantum) inductor³⁸. In fact, the emergent inductance signal was recently observed by some of us in $\text{Gd}_3\text{Ru}_4\text{Al}_{12}$ ³⁹, exploring the zero-field helical (HE) phase – discussed above – as a prototypical spiral order of large local moments coupled to the Fermi sea. The present model indicates that the spiral plane in $\text{Gd}_3\text{Ru}_4\text{Al}_{12}$ is easily depinned and rotated, enabled

by a balance of anisotropic exchange and local-ion anisotropy. This property facilitates spin dynamics, helping to make the emergent electric field observable in transport experiments. Beyond shedding light on the issue of skyrmion formation, we hope that our work can guide the ongoing search for room-temperature material hosts of the emergent inductance effect.

Acknowledgments. We acknowledge discussions with J. Masell and T.-h. Arima. S. H. benefited from support by JSPS KAKENHI Grants Numbers JP18K13488, JP19K03752, and JP19H01834. This work was partially supported by JST CREST Grant Number JP-MJCR1874 (Japan).

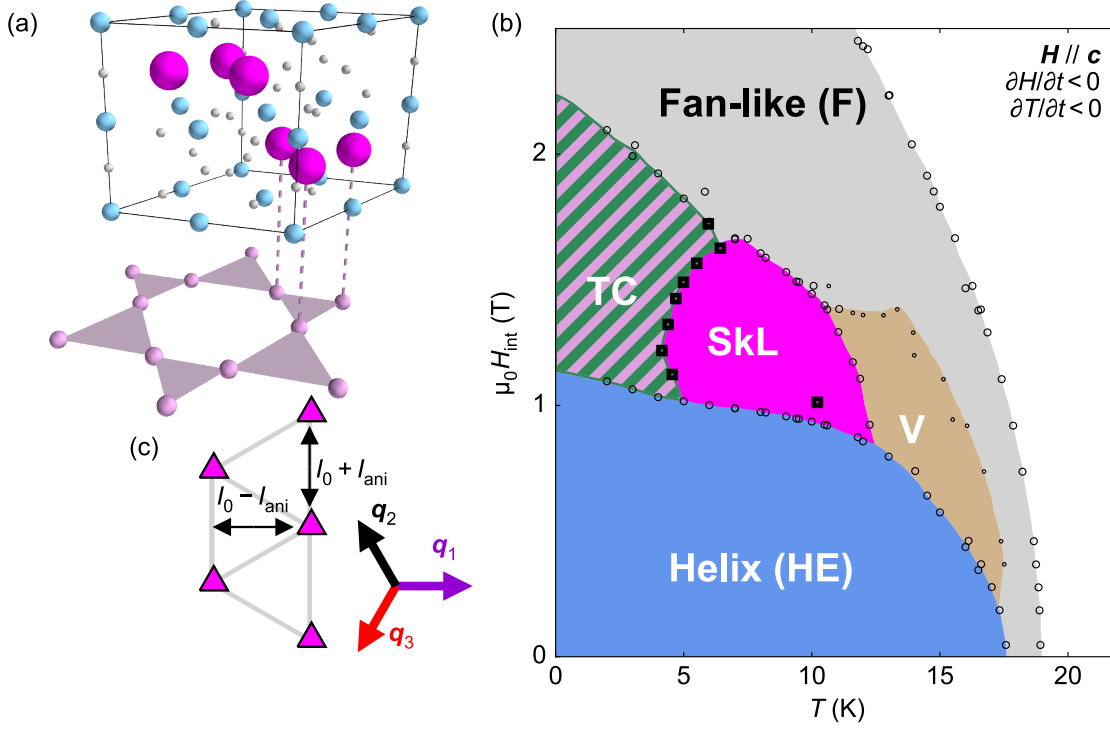
* hirschberger@ap.t.u-tokyo.ac.jp

1. T. Okubo, S. Chung, and H. Kawamura, “Multiple- q states and the skyrmion lattice of the triangular-lattice Heisenberg antiferromagnet under magnetic fields,” *Phys. Rev. Lett.* **108**, 017206 (2012).
2. A.O. Leonov and M. Mostovoy, “Multiply periodic states and isolated skyrmions in an anisotropic frustrated magnet,” *Nature Communications* **6**, 8275 (2015).
3. R. Ozawa, S. Hayami, and Y. Motome, “Zero-field skyrmions with a high topological number in itinerant magnets,” *Physical Review Letters* **118**, 147205 (2017).
4. S. Hayami, R. Ozawa, and Y. Motome, “Effective bilinear-biquadratic model for noncoplanar ordering in itinerant magnets,” *Physical Review B* **95**, 224424 (2017).
5. Z. Wang, Y. Su, S.-Z. Lin, and C.D. Batista, “Skyrmion crystal from RKKY interaction mediated by 2D electron gas,” *Physical Review Letters* **124**, 207201 (2020).
6. T. Shimokawa and H. Kawamura, “Ripple state in the frustrated honeycomb-lattice antiferromagnet,” *Phys. Rev. Lett.* **123**, 057202 (2019).
7. V. Lohani, C. Hickey, J. Masell, and A. Rosch, “Quantum skyrmions in frustrated ferromagnets,” *Physical Review X* **9**, 041063 (2019).
8. T. Kurumaji, T. Nakajima, M. Hirschberger, A. Kikkawa, Y. Yamasaki, H. Sagayama, H. Nakao, Y. Taguchi, T.-h. Arima, and Y. Tokura, “Skyrmion lattice with a giant topological Hall effect in a frustrated triangular-lattice magnet,” *Science* **365**, 914–918 (2019).
9. M. Hirschberger, T. Nakajima, S. Gao, L. Peng, A. Kikkawa, T. Kurumaji, M. Kriener, Y. Yamasaki, H. Sagayama, H. Nakao, K. Ohishi, K. Kakurai, Y. Taguchi, X. Yu, T.-h. Arima, and

- Y. Tokura, “Skyrmion phase and competing magnetic orders on a breathing kagomé lattice,” *Nature Communications* **10**, 5831 (2019).
10. S. Gao, O. Zaharko, V. Tsurkan, Y. Su, J.S. White, G.S. Tucker, B. Roessli, F. Bourdarot, R. Sibille, D. Chernyshov, T. Fennell, A. Loidl, and C. Rüegg, “Spiral spin-liquid and the emergence of a vortex-like state in MnSc_2S_4 ,” *Nature Physics* **13**, 157–161 (2017).
 11. S. Gao, H.D. Rosales, F.A. Gómez Albarracín, V. Tsurkan, G. Kaur, T. Fennell, P. Steffens, M. Boehm, P. Čermák, A. Schneidewind, E. Ressouche, D.C. Cabra, C. Rüegg, and O. Zaharko, “Fractional antiferromagnetic skyrmion lattice induced by anisotropic couplings,” *Nature* **586**, 37–41 (2020).
 12. I. E. Dzyaloshinskii, “Thermodynamical theory of ‘weak’ ferromagnetism in antiferromagnetic substances,” *Sov. Phys. JETP* **5**, 1259 (1957).
 13. Tôru Moriya, “Anisotropic superexchange interaction and weak ferromagnetism,” *Physical Review* **120**, 91–98 (1960).
 14. P. Bak and M.H. Jensen, “Theory of helical magnetic structures and phase transitions in MnSi and FeGe ,” *Journal of Physics C: Solid State Physics* **13**, L881–L885 (1980).
 15. U. K. Röbner, A. N. Bogdanov, and C. Pfleiderer, “Spontaneous skyrmion ground states in magnetic metals,” *Nature* **442**, 797–801 (2006).
 16. A. Kitaev, “Anyons in an exactly solved model and beyond,” *Annals of Physics* **321**, 2–111 (2006).
 17. G. Jackeli and G. Khaliullin, “Mott insulators in the strong spin-orbit coupling limit: From Heisenberg to a quantum compass and Kitaev models,” *Physical Review Letters* **102**, 017205 (2009).
 18. R. E. Gladyshevskii, O. R. Strusievicz, K. Cenzual, and E. Parthé, “Structure of $\text{Gd}_3\text{Ru}_4\text{Al}_{12}$, a new member of the $\text{EuMg}_{5.2}$ structure family with minority-atom clusters,” *Acta Crystallographica Section B* **49**, 474–478 (1993).
 19. J. Niermann and W. Jeitschko, “Ternary rare earth (R) transition metal aluminides $R_3T_4\text{Al}_{12}$ ($T = \text{Ru}$ and Os) with $\text{Gd}_3\text{Ru}_4\text{Al}_{12}$ type structure,” *Journal for Inorganic and General Chemistry* **628**, 2549–2556 (2002).
 20. V. Chandragiri, K. K. Iyer, and E.V. Sampathkumaran, “Magnetic behavior of $\text{Gd}_3\text{Ru}_4\text{Al}_{12}$, a layered compound with distorted kagomé net,” *Journal of Physics: Condensed Matter* **28**, 286002 (2016).

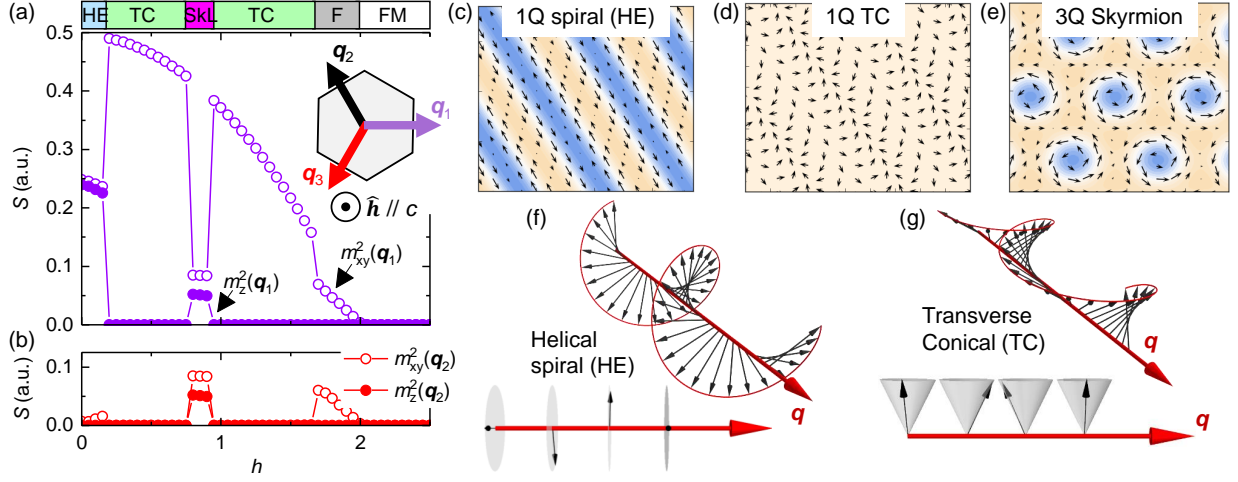
21. T. Matsumura, Y. Ozono, S. Nakamura, N. Kabeya, and A. Ochiai, “Helical ordering of spin trimers in a distorted Kagome lattice of $\text{Gd}_3\text{Ru}_4\text{Al}_{12}$ studied by resonant x-ray diffraction,” *J. Phys. Soc. Jpn.* **88**, 023704 (2019).
22. S. Nakamura, N. Kabeya, M. Kobayashi, K. Araki, K. Katoh, and A. Ochiai, “Spin trimer formation in the metallic compound $\text{Gd}_3\text{Ru}_4\text{Al}_{12}$ with a distorted kagome lattice structure,” *Physical Review B* **98**, 054410 (2018).
23. Y.-D. Li, X. Wang, and G. Chen, “Anisotropic spin model of strong spin-orbit-coupled triangular antiferromagnets,” *Physical Review B* **94**, 035107 (2016).
24. S. Hayami and Y. Motome, “Néel- and Bloch-type magnetic vortices in Rashba metals,” *Physical Review Letters* **121**, 137202 (2018).
25. F.N. Rybakov, A.B. Borisov, S. Blügel, and N.S. Kiselev, “New spiral state and skyrmion lattice in 3D model of chiral magnets,” *New Journal of Physics* **18**, 045002 (2016).
26. P. Puphal, V. Pomjakushin, N. Kanazawa, V. Ukleev, D. J. Gawryluk, J. Ma, M. Naamneh, N. C. Plumb, L. Keller, R. Cubitt, E. Pomjakushina, and J. S. White, “Topological magnetic phase in the candidate weyl semimetal cealges,” *Physical Review Letters* **124**, 017202 (2020).
27. T. Nomoto, T. Koretsune, and R. Arita, “Formation mechanism of the helical \mathbf{Q} structure in Gd-based skyrmion materials,” *Phys. Rev. Lett.* **125**, 117204 (2020).
28. *Supplementary Information.*
29. P. Bruno, V.K. Dugaev, and M. Taillefumier, “Topological Hall effect and Berry phase in magnetic nanostructures,” *Phys. Rev. Lett.* **93**, 096806 (2004).
30. A. Neubauer, C. Pfleiderer, B. Binz, A. Rosch, R. Ritz, P.G. Niklowitz, and P. Böni, “Topological Hall effect in the A phase of MnSi ,” *Phys. Rev. Lett.* **102**, 186602 (2009).
31. R. Ritz, M. Halder, C. Franz, A. Bauer, M. Wagner, R. Bamler, A. Rosch, and C. Pfleiderer, “Giant generic topological Hall resistivity of MnSi under pressure,” *Phys. Rev. B* **87**, 134424 (2013).
32. N. Nagaosa, J. Sinova, S. Onoda, A.H. MacDonald, and N.P. Ong, “Anomalous Hall effect,” *Rev. Mod. Phys.* **82**, 1539–1592 (2010).
33. R. Karplus and J. M. Luttinger, “Hall effect in ferromagnetics,” *Physical Review* **95**, 1154 (1954).
34. M. Lee, Y. Onose, Y. Tokura, and N. P. Ong, “Hidden constant in the anomalous hall effect of high-purity magnet mnsi ,” *Phys. Rev. B* **75**, 172403 (2007).

35. S. Hayami, S.-Z. Lin, and C.D. Batista, “Bubble and skyrmion crystals in frustrated magnets with easy-axis anisotropy,” *Phys. Rev. B* **93**, 184413 (2016).
36. S. Bordács, A. Butykai, B. G. Szigeti, J. S. White, R. Cubitt, A. O. Leonov, S. Widmann, D. Ehlers, H.-A. Krug von Nidda, V. Tsurkan, A. Loidl, and I. Kézsmárki, “Equilibrium skyrmion lattice ground state in a polar easy-plane magnet,” *Scientific Reports* **7**, 7584 (2017).
37. A. O. Leonov and I. Kézsmárki, “Skyrmion robustness in noncentrosymmetric magnets with axial symmetry: The role of anisotropy and tilted magnetic fields,” *Physical Review B* **96**, 214413 (2017).
38. N. Nagaosa, “Emergent inductor by spiral magnets,” *Jpn. J. Appl. Phys.* **58**, 12 (2019).
39. T. Yokouchi, F. Kagawa, M. Hirschberger, Y. Otani, N. Nagaosa, and Y. Tokura, “Emergent electromagnetic induction in a helical-spin magnet,” *Nature* **586**, 232–236 (2020).



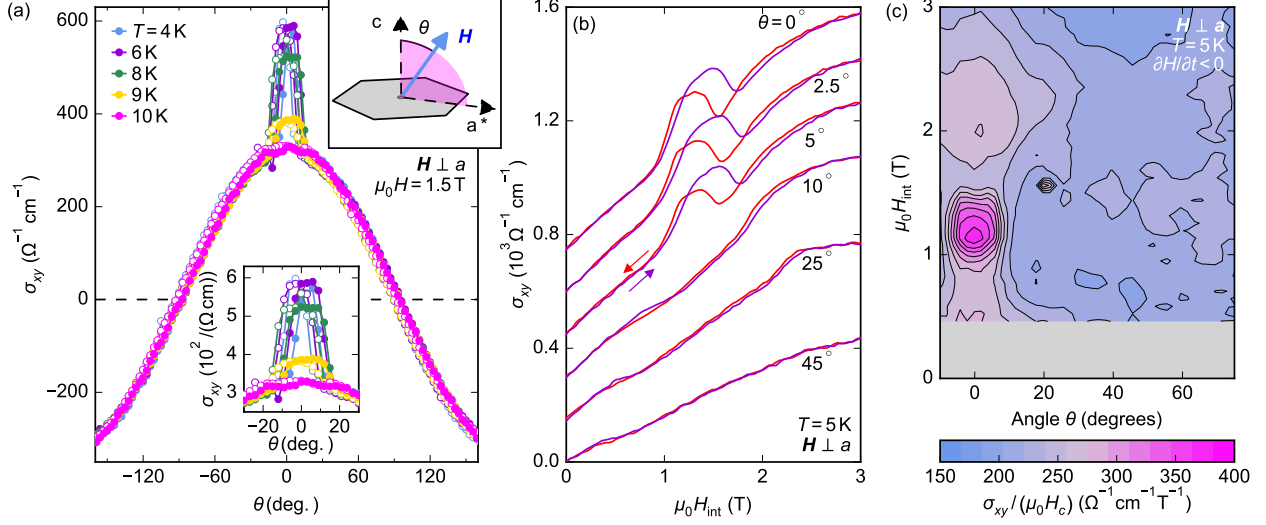
1

2 FIG. 1. (color online). Magnetic interactions in centrosymmetric $Gd_3Ru_4Al_{12}$. (a) Hexagonal crys-
 3 tal structure with Al, Ru, and Gd atoms marked by white, blue, and magenta spheres, respectively.
 4 (b) Magnetic phase diagram for magnetic field applied along the c -axis. (c) The distorted Kagome
 5 motif of rare earth sites is approximated as a triangular lattice of trimer plaquettes (magenta tri-
 6 angles). Three possible directions, equivalent by symmetry, of the magnetic ordering vector \mathbf{q}_ν
 7 ($\nu = 1, 2, 3$) are indicated in the figure. Specifically for \mathbf{q}_1 , we illustrate the anisotropy of parallel
 8 and perpendicular magnetic exchange interactions by black arrows. Data points in (b) adopted
 9 from Ref.⁹.



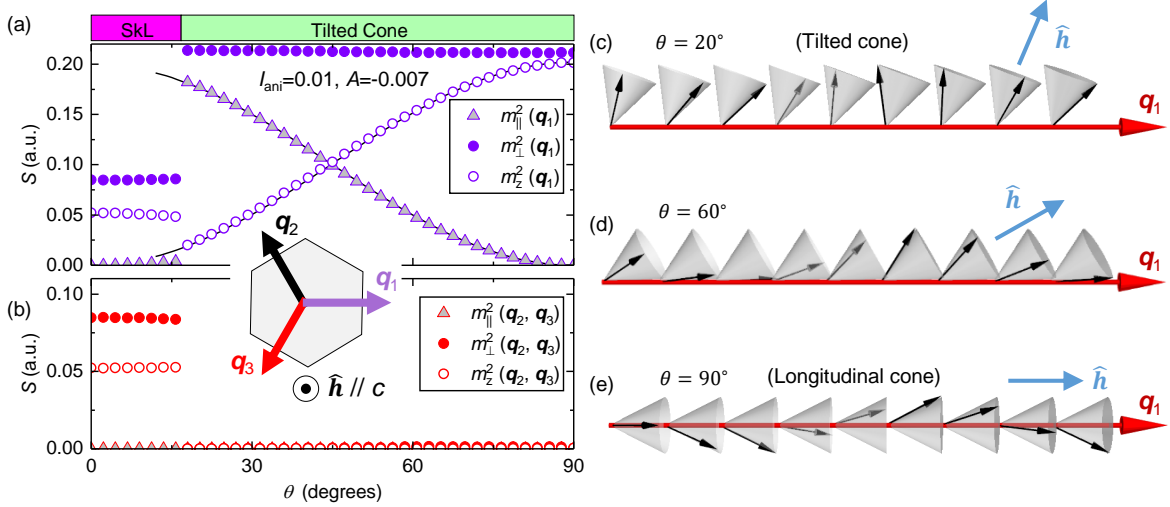
10

11 FIG. 2. (color online). Simulated-annealing of magnetic order on the triangular lattice, for magnetic
 12 field $\hat{\mathbf{h}} \parallel c$. h is the magnitude of the applied magnetic field measured in units of the exchange
 13 coupling J . (a,b), Components of the magnetic structure factor $S_\alpha(\mathbf{q}_\nu) \sim m_\alpha^2(\mathbf{q}_\nu)$, where $m_\alpha(\mathbf{q}_\nu)$
 14 is a vector component of the modulated magnetic moment at \mathbf{q}_ν with $\nu = 1, 2$. The simulated
 15 annealing calculation is carried out²⁸ for parameters $I_{\text{ani}} = 0.01$, $A = -0.007$ at low temperature
 16 $T = 0.01 \cdot J$. Inset of (a), the three-fold degeneracy of the \mathbf{q}_ν in the hexagonal plane. Colored
 17 bands at the top define parameter regimes for phases HE (helical), TC (transverse conical), SkL
 18 (skyrmion lattice), F (fan-like), and field-aligned ferromagnet (FM). In (c-e) magnetic textures are
 19 shown by arrows (magnetic moment in the hexagonal plane) and the color map, where yellow and
 20 blue correspond to positive and negative c -component of the moment, respectively. In (f,g) we
 21 depict both a three-dimensional sketch of the orders in phases HE and TC, and an illustration in
 22 terms of spiral planes and cones (lower side).



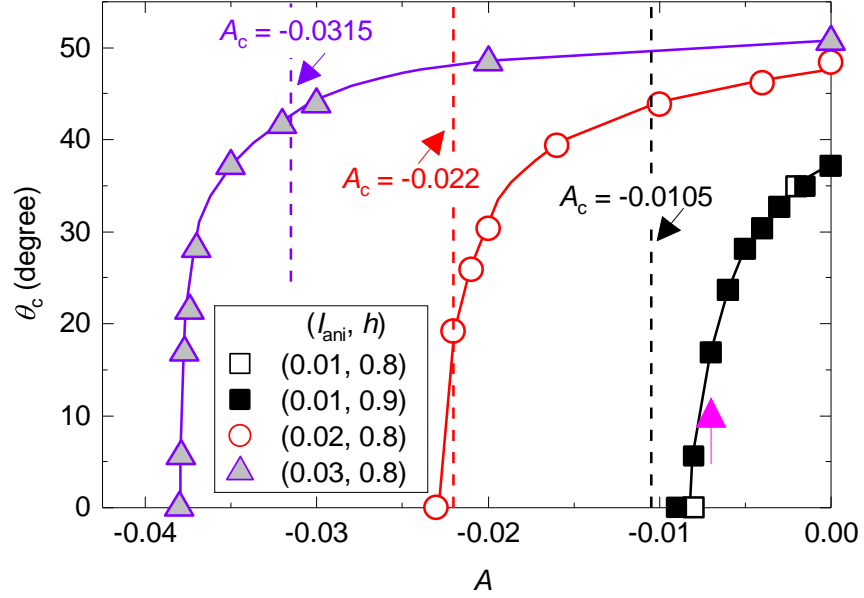
23

24 FIG. 3. (color online). Collapse of skyrmion lattice (SkL) in $\text{Gd}_3\text{Ru}_4\text{Al}_{12}$ upon slight tilting of
 25 the magnetic field, as detected experimentally by the topological Hall effect. (a) Angle-dependent
 26 Hall conductivity σ_{xy} at fixed magnetic field and temperature ($\mu_0 H = 1.5\text{T}$). Open and solid
 27 symbols mark decreasing and increasing angle θ . The right-hand and bottom insets illustrate
 28 the experimental geometry and show an expanded view of the data, respectively. (b) Field scan
 29 of σ_{xy} at fixed θ . Red and violet curves are for decreasing and increasing field, marked by the
 30 arrows. (c) The region of enhanced intensity in the contour map of $\sigma_{xy}/(\mu_0 H_c)$ is identified with
 31 the SkL phase. $H_c = H \cos \theta$ is the component of the magnetic field parallel to the c -axis. A
 32 demagnetization correction was applied to obtain the internal magnetic field $\mu_0 H_{\text{int}}$ for panels
 33 (b,c).



34

35 FIG. 4. (color online). Modeling of tilting-induced destruction of the skyrmion lattice. (a,b)
 36 Components of the magnetic structure factor $S_{\mathbf{q}_\nu}$ for two reflections \mathbf{q}_ν at $h = 0.8$ (c.f. Fig. 2).
 37 For this parameter set, the SkL collapses at tilt angle $\theta_c \approx 15^\circ$. In (a), the black solid lines show
 38 that $m_{\parallel}^2 \sim \cos^2 \theta$ and $m_z^2 \sim \sin^2 \theta$ for $\theta > \theta_c$, respectively. (c-e) conical order at $\theta > \theta_c$, where the
 39 axis $\hat{\mathbf{n}}_1$ of the cone at \mathbf{q}_1 smoothly follows the direction of the magnetic field.



40

41 FIG. 5. (color online). Critical angle θ_c of the skyrmion lattice and its dependence on model
 42 parameters. For each $I_{\text{ani}} = 0.01, 0.02, 0.03$, a vertical line indicates the limit of stability for the
 43 helical (HE) state in zero magnetic field. When $A < A_c$, the $h = 0$ ground state is transverse conical
 44 (TC). The parameters chosen for $\text{Gd}_3\text{Ru}_4\text{Al}_{12}$ are marked by a magenta arrow. For $I_{\text{ani}} = 0.01$,
 45 two different values of the applied field h – normalized by exchange constant J – are used for the
 46 simulation, demonstrating the robustness of the result (solid and open squares). The lines passing
 47 through the data points are a guide to the eye.